Physica Medica 124 (2024) 103420

Contents lists available at ScienceDirect

Physica Medica

journal homepage: www.elsevier.com/locate/ejmp

Preclinical photon minibeam radiotherapy using a custom collimator: Dosimetry characterization and preliminary in-vivo results on a glioma model

Canan Koksal Akbas [a,b,1], Federica Vurro [a,1], Claudio Fiorino [c,*], Cesare Cozzarini [d], Francesco Cavaliere [e], Paolo Milani [e], Sara Broggi [c], Antonella Del Vecchio [c], Nadia Di Muzio [d], Carlo Tacchetti [a], Antonello Enrico Spinelli [a]

[a] Experimental Imaging Center, IRCCS San Raffaele Scientific Institute, Milan, Italy
[b] Medical Physics Department, Istanbul University Oncology Institute, Istanbul, Turkey
[c] Medical Physics Department, IRCCS San Raffaele Scientific Institute, Milan, Italy
[d] Radiotherapy Department, IRCCS San Raffaele Scientific Institute, Milan, Italy
[e] Department of Physics, University of Milan, Milan, Italy

ARTICLE INFO

Keywords:
Minibeam radiotherapy
Monte Carlo simulations
Film dosimetry

ABSTRACT

Purpose: The purpose of this study is to investigate the dosimetric characteristics of a collimator for minibeam radiotherapy (MBRT) with film dosimetry and Monte Carlo (MC) simulations. The outcome of MBRT with respect to conventional RT using a glioma preclinical model was also evaluated.
Methods: A multi-slit collimator was designed to be used with commercial small animal irradiator. The collimator was built by aligning 0.6 mm wide and 5 mm thick parallel lead leaves at 0.4 mm intervals. Dosimetry characteristics were evaluated by Gafchromic (CG) films and TOPAS Monte Carlo (MC) code.
An in vivo experiment was performed using a glioma preclinical model by injecting two million GL261cells subcutaneously and treating with 25 Gy, single fraction, with MBRT and conventional RT. Survival curves and acute radiation damage were measured to compare both treatments.
Results: A satisfactory agreement between experimental results and MC simulations were obtained, the measured FWHM and distance between the peaks were respectively 0.431 and 1.098 mm.
In vivo results show that MBRT can provide local tumor control for three weeks after RT treatment and a similar survival fraction of open beam radiotherapy. No severe acute effects were seen for the MBRT group.
Conclusions: We developed a minibeam collimator and presented its dosimetric features. Satisfactory agreement between MC and GC films was found with differences consistent with uncertainties due to fabrication and set-up errors. The survival curves of MBRT and open field RT are similar while atoxicity is dramatically lower with MBRT, preliminarily confirming the expected effect.

1. Introduction

Radiotherapy (RT) aims to deliver curative doses to the tumor precisely while sparing surrounding healthy organs. Although the sparing of normal tissues dramatically improved thanks to sophisticated beam delivery methods combined with accurate image-guidance systems, treatment-related adverse effects are still among the major limiting factors of RT efficacy [1]. For example, the delivery of high doses required to eradicate aggressive brain tumors without exceeding the tolerance limit for the surrounding brain tissue and for other organs like optical nerves, chiasma and brainstem is a challenging issue [2]. Therefore, the treatment of these tumors cannot be curative.

Novel preclinical approaches have been developed to reduce normal tissue complication such as micro beam (MRT) or mini beam radiotherapy (MBRT) [3]. MRT or MBRT are referred as spatially fractionated technique. The fundamental principle is based on the reduction of the

* Corresponding author.
E-mail address: fiorino.claudio@hsr.it (C. Fiorino).
[1] **Co-first authors.**

https://doi.org/10.1016/j.ejmp.2024.103420
Received 1 February 2024; Received in revised form 28 May 2024; Accepted 28 June 2024
Available online 5 July 2024

irradiated normal tissue volume to increase radiation tolerance, although the mechanisms behind MRT/MBRT effects have not been yet fully understood [4,5]. In general, for MRT, kilovoltage X-ray beams delivered by a synchrotron source of 25–100 μm size separated by 100–400 μm intervals are used to generate a spatially fractionated dose distribution [6]. Unlike standard RT, this beam configuration results in non-uniform dose profiles composing of high and low dose regions defined as peaks and valleys. The peak dose is the dose at the center of the beam while the valley dose is the minimum dose between two consecutive beams. The peak-to-valley dose ratio (PVDR) is usually considered a the key dosimetric parameter of spatially fractionated RT (SFRT) where higher PVDR's have shown to yield reduced toxicities [3,7]. Therefore, major efforts have been made to maximize PVDR. However, a recent comprehensive review has highlighted a strong correlation between valley dose and increased life span in preclinical SFRT experiments [8]. Therefore, it may not be necessary to have a high PVDR, and, thus, potentially permitting the delivery of SFRT modalities with MV energies used in the clinic.

In preclinical MRT animal experiments performed at synchrotron facilities, radiation dose (peak dose) of hundreds of Gy in a single fraction were well tolerated by a range of normal tissues [9,10,11]. At the same time the valley dose must be less than the tissue tolerance level to broad beams in order to maintain the sparing effect of MRT [7]. Importantly, MRT seems to enable a remarkable tumor control in radioresistant tumors although a significant part of the tumor volume is exposed to a lower dose [7,12]. Such very high doses are delivered in a short time to avoid beam smearing due to tissue motion. At the moment, only synchrotron sources are capable of producing ultra-high dose rates MRT, making also impossible to decouple spatial from temporal (FLASH) effects.

The dimensions of a typical preclinical beam size used for MBRT ranges between 100 μm to 1 mm with a beam spacing of up to 4 mm obtained by collimating larger beam sizes. Dilmanian et al [13] investigated the healthy tissue tolerance of MBRT on a rat model. No side effects were observed up to 170 Gy peak dose delivered to the brain using 0.68 mm sized minibeams (spaced 1.36 mm on center), the in-depth integrated dose was 88 Gy.

Prezado et al [14] performed experiments with minibeams of 0.6 mm (1.2 mm center to center distance) and found that the rat brain tolerated a peak dose of 100 Gy (and a valley dose of 6.6 Gy) in one fraction. Additionally, animal studies demonstrated the significant delay in tumor growth of radioresistant tumor treated with MBRT [14,15]. These results suggested that MBRT might be an alternative to MRT, with the main advantage that MBRT may be delivered more easily, in principle using preclinical irradiator based on conventional x-ray sources. Secondly, except for tumors located in the diaphragm/lungs regions, the MBRT dose distributions are generally less prone to beam blurring due to organ movements with respect to MRT. These interesting features of MBRT open the door to carrying out more MBRT preclinical experiments.

As mentioned before, the limited availability of synchrotron sources and the promising results from MBRT studies pushed the implementation of MBRT in preclinical facilities equipped with small animal irradiators. Bablock et al [16] designed a collimator model comprising of 0.8 mm tungsten leaves separated by 1 mm gaps for an orthovoltage X-ray machine. A comparison between MC simulations and film measurement was performed showing that the designed collimator may be used for MBRT experiments. Hadsell et al [17] obtained minibeams with a width of 0.3 mm using carbon nanotube X-ray technology. Prezado et al [18] made major modifications of the Small Animal Radiation Research Platform (SARRP) to deliver MBRT. They developed a collimator with a length of 10.23 cm that can be used instead of the standard collimator. The tip of this collimator has seven divergent slits with central slit a width of 0.4 mm to create a minibeams pattern. In their study, the dosimetry of minibeams were carried out before performing radiobiological experiments and a good agreement between experimental and simulations results were found. Bayzar et al [19] generated MBRT beams using a small animal irradiator (X-RAD 320, PXi); in order to obtain a narrow penumbra, they placed the minibeam collimator, consisting of 0.3 mm slits and 0.6 mm lead ribbon, adjacent to the target and increased the focus surface distance (FSD).

The main goal of our work was the development and the dosimetric characterization of a compact secondary parallel minibeam collimator that can be easily attached to the conventional primary broad beam collimators of our dedicated image guided small animal irradiator (X-RAD225Cx SmART, PXI, North Branford, CT, USA). The main advantage of such an approach is that different minibeam fields shape (e.g. 10x10 mm^2, 20x20 mm^2 etc.) could be obtained using the same secondary collimator. Secondly, using this tool it will be also possible to use several minibeam collimator inserts with different beam and valley size. Overall, our approach is also cost effective since it will not be necessary to build entirely new collimators for MBRT. In order to develop an MC model that could be used for further MBRT optimization, we first built a model of our small animal irradiator considering conventional broad beam fields. In this step, particular attention has been focused to the x-ray source, primary collimators design and validation using radiochromic films. We then performed preliminary MC simulations of our prototype MBRT collimator.

Finally, as a first proof of principle, we evaluated in vivo the outcome of MBRT with respect to broad beam RT using a glioma preclinical model. Survival curves and acute radiation damage were measured to compare both treatments.

2. Materials and methods

2.1. X-ray source

A dedicated small animal irradiator (X-RAD225Cx SmART, PXI, North Branford, CT, USA) available at the San Raffaele Scientific Institute Preclinical Imaging Facility was used as an X-ray source. The XRAD-SmART system uses a dual focal-spot X-ray tube mounted on a rotational C-arm gantry with focal spot sizes of 5.5 mm and 0.4 mm for treatment and imaging, respectively. The tube potential of 225 kVp and current of 13 mA with 2 mm Beryllium inherent and 0.3 mm Cu additional filters are employed for treatment. The beam calibration is performed at source-to-isocenter distance of 30.7 cm. The system is equipped with 9 collimators shaping 1-, 2-, 3-, and 5-mm diameter circular beams, 10x10 mm^2, 20x20 mm^2, and 40x40 mm^2 square beams, and 10x30 mm^2 and 30x40 mm^2 rectangular beams.

2.2. Custom mini beam collimator design

An in-house secondary parallel minibeam collimator (MBC) was built to obtain a minibeam pattern. The multi-slit collimator was built by aligning 0.6 mm wide and 5 mm thick lead leaves parallel to each other at 0.4 mm intervals.

Lead, considering its high density and a high atomic number, is one of the best materials to shield x-rays and is commonly used to manufacture collimators for different nuclear medicine imaging (SPECT) or preclinical radiotherapy applications [20].

High-density plastic material (polyethylene terephthalate) was used as a spacer material. The dimensions of the MBC insert were 40x40 mm^2. We also designed an auxiliary tool to easily mount and align the MBC to the standard (primary) collimator. The tool has a square aperture where MBC with different beam and valley size can be inserted (Fig. 1). This secondary MBC can be easily attached and aligned to any standard primary; therefore, measurements can be carried out in the desired field size.

2.3. Dosimetry

Absolute and relative dosimetry measurements were performed.

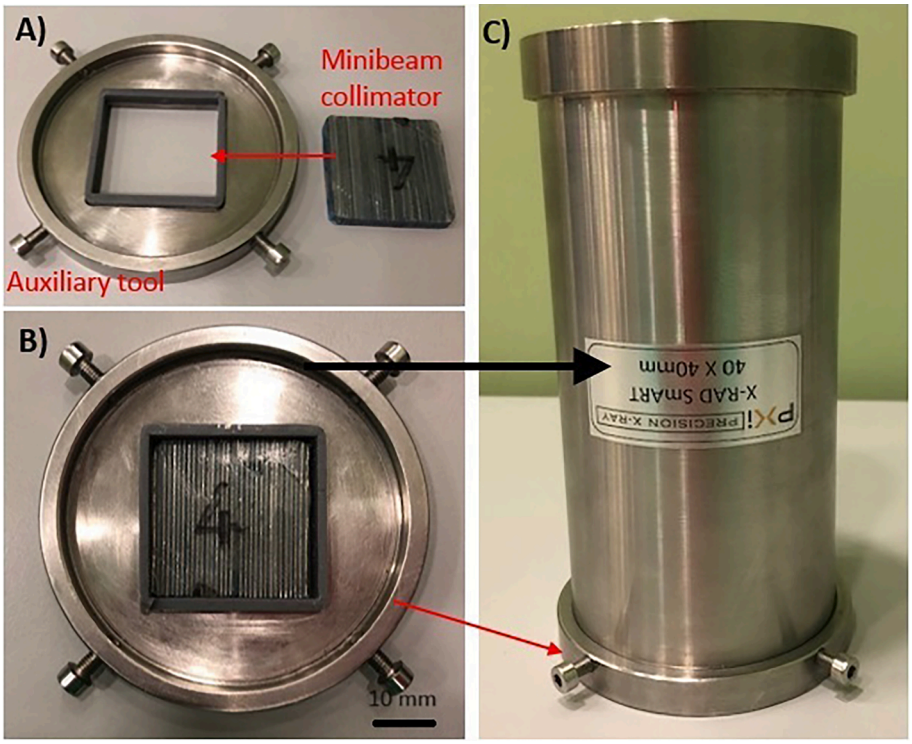

Fig. 1. A) The minibeam collimator (MBC) and the auxiliary tool. B) The MBC is inserted into the tool. C) The MBC is mounted to the standard collimator.

First, absolute dose measurements for the unmodulated (broad) beam were carried out using a Farmer-type ion chamber using the same irradiator commissioning setup. The measurements were made with the chamber placed at the phantom (10x10x2 cm^3) surface for 40x40 mm2 field size at SID = 30.7 cm. Dose was measured following the AAPM TG-61 protocol [21].

Dosimetry of minibeams was performed using Gafchromic (GC) EBT3 films (lot number 01042102). GC film consists of a single active layer, 28 μm thick, sandwiched between two transparent polyester sheets with a thickness of 125 μm.

GC films were calibrated similarly to Spinelli et al ([22]). In short, films were irradiated to doses up to 10 Gy in a 40x40 mm^2 field. Films were scanned in the same orientation using an Epson 10000XL scanner at: 800dpi resolution, 48-bit color depth 24 h after irradiation. Optical density (OD) of the red-channel images was used for calibration. The dose–response data were fitted to a 3rd order polynomial function and the resulting calibration curve was then used to convert OD to dose.

The relatively large focal spot size of the X-ray tube causes a wider penumbra that can affect the MBC output, resulting in a smoother peak-valley dose pattern. The penumbra effect can be reduced if the collimator to target distance decreases (Fig. 2-A), therefore all irradiations were made just under the collimators with less than 1 mm gap between the collimator and the phantom. The same setup and small distance have been used for irradiation of cells and small animals.

In order to measure the output factor (OF), GC films with a size of 3x3 cm^2 were irradiated for 60 s using mini beams and 20x20 mm^2 open collimator. Dose measurements were then performed by taking the mean value of a central 10x10 mm^2 square region of interest (ROI) on the irradiated films.

The OF was assessed as the ratio of the average dose measured by GC film irradiated using MBC with respect to the corresponding open field, at the phantom surface.

GC film irradiations were repeated 5 times: the peak valley dose ratio (PVDR), beam size (full width half maximum = FWHM), and distance

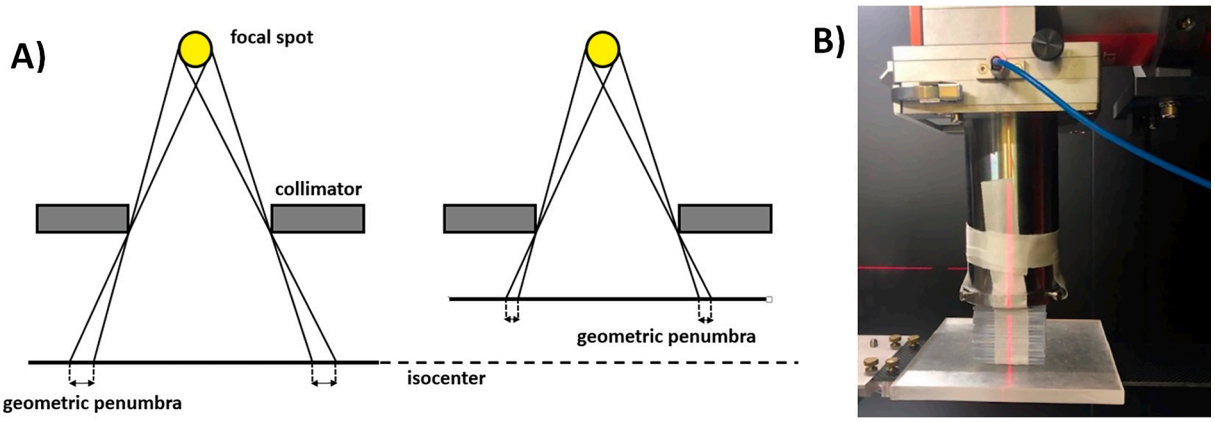

Fig. 2. A) Demonstration of large (left) and small (right) geometric penumbra associated with collimator-to-target distance. B) Setup for PDD measurement for minibeams.

between peaks were measured for each of the resulting five films. The PVDR is defined as:

$$PVDR = \frac{Peakdose}{Valleydose} \quad (1)$$

The distance between peaks, and FWHM were assessed as the mean values of the five measurements with the corresponding SD calculated accordingly. All these parameters were measured in the central part of the MB pattern (five adjacent central beams).

PMMA slabs with a size of 50x50x2.12 mm^3 were used to measure the percentage depth dose (PDD) of both broad and mini beams. The PDD measurements were performed by placing GC films, starting from the phantom surface, between sixteen PMMA slabs (Fig. 2-B). The dependence of the PVDR and FWHM with respect to depth was determined from EBT3 films dose profiles. The thickness of film (0.278 mm) was considered for PDD measurement. In-house written Matlab scripts were used for the analyses.

2.4. Monte Carlo simulations setup

As mentioned in the introduction, we also developed an MC toolbox that could be used for optimizing MBRT collimators geometries and materials.

In the first step (see section 2.4.1) we implemented a model of our small animal irradiator considering a conventional (open beam) radiotherapy setup. Secondly, as described in section 2.4.2, we carried out preliminary MC simulations of MBRT using the same geometry and material of the collimator prototype described in section 2.2.

All the simulations were performed using the TOPAS v 3.8.1 MC code based on Geant4 v geant4.10.07.p03 [23].

2.4.1. Monte Carlo model of the SmART irradiator

Instead of simulating the X-ray tube in detail, a virtual X-ray source was modeled at the effective focal spot position. A nominal focal spot size equal to 5.5 mm diameter and beam divergence (40°) provided by the manufacturer were used. The energy spectrum was calculated by SpekCalc using the manufacturer information [24–26]. The standard collimators 10x10 mm^2, 20x20 mm^2, and 40x40 mm^2 were also modeled and the "g4em-standard_opt4" physics list was implemented. The cut for all particles was set to 1 μm without any variance reduction techniques. The dose to medium was scored in a 0.5x0.5x1 mm^3 voxels for the dose profiles (DP) at the PMMA phantom surface. The voxel was equal to 0.1x1x0.1 mm^3 for the depth doses (DD) simulation using the 40x40 mm^2 collimator (PMMA slabs, 2.12 mm thickness and polyester slab = 0.278). A total of $3x10^{11}$ and $4.5x10^{11}$ primary photons were simulated for the DP and DD, respectively. The MC simulations were performed on a High Performance Computing (HPC) platform composed by 17 CPU nodes XL190r Gen10 equipped with Intel® Xeon® Gold 6240 @2.6 GHz 24.75 MB with 36 cores and 384 GB of memory each. Moreover, a Nvidia® dgx01® equipped with 8 V100, Intel® Xeon® E5-2698 @2.20Ghz 50 MB and 512 GB of memory is present. Storage is composed by 1) the parallel distributed filesystem beegfs® composed by 8 Apollo 4200 Gen10 for a grand total of 1.02 PB and 2) by the qumulo® distributed filesystem composed by 7 Apollo 4200 Gen 9 90 TB for a grand total of 474.8 TB.

The results of the MC simulations were compared against GC dosimetry, including FWHM, geometric penumbra, and PDD measurements (see section 2.3).

Considering that it is not straightforward to accurately define landmarks on both MC and GC films, rigid registration between the two has been performed using the intensity based automatic image registration routine implemented in Matlab. The rigid transformation was calculated by minimizing the mean square difference between the normalized MC and GC films.

2.4.2. Monte Carlo model of the minibeam collimator

After the verification of the SmART MC model with broad beam data, the MBRT MC simulations were carried out.

The simulated MBC has the same dimensions as our prototype consisting of 0.6 mm gaps and 0.4 mm lead slits. The spacer material considered in the simulations was polyethylene terephthalate (PET, ρ = 1.38 g/cm^3). In all simulations, the dose to medium in the PMMA phantom was scored with 0.1x1x0.1 mm^3 voxel sizes and $4.5x10^{11}$ primary histories were simulated using 1 μm cut range for all particles. Using this setup, the uncertainties of dose calculation were equal to 2 % and simulation time was about 48 h.

The simulated OF, peak PDD, PVDR, and FWHM were compared with the experimental data obtained with GC film.

2.5. In vivo conventional and MBRT of a glioma preclinical model

The outcome of MBRT with respect to broad beam RT was evaluated in vivo using a glioma preclinical model performed by injecting two million GL261cells subcutaneously into the left flank near the leg of 30 C57BL/6 mice (weight 17–23 g).

The mice were anesthetized and treated in the supine position as follows: 10 received 25 Gy, single fraction conventional RT, 10 mice received 25 Gy mean dose (peak dose = 56 Gy, valley dose = 4 Gy), single fraction MBRT and 10 mice were used as control unirradiated group. Both conventional and MBRT treatments were performed using one single beam (anterior posterior) to keep the same radiation geometry.

The mice were treated when the tumor size was equal to about 150 mm^3 and sacrificed when the tumor was larger than 1500 mm^3 or when the side effects induced by RT were very severe and incompatible with life due to pain. The tumor volume was measured every 3–4 days using a caliper for up to 45 days after radiotherapy.

Accordingly to Soto et al [27] an ordinal scale to score skin toxicity was developed using the following criteria: A score of 0 = normal (null); 1 = depigmentation or Alopecia within the radiation field (mild); 2 = Desquamation within the radiation field (moderate); 3 = ulceration (±alopecia and depigmentation) within the radiation field (severe); All mice were scored by two independent observers blinded to the intervention. If scores deviated between observers, the average of the two scores were used as the final score.

3. Results

3.1. Dosimetry of open field and comparison with MC simulations

The dose rate measured with a farmer-type ion chamber was found to be 3.86 Gy/min for a 40x40 mm^2 broad beam at the isocenter. The mean dose rate measured with GC for the standard collimator 20x20 mm^2 and MBC were 5.6 ± 0.1 Gy/min and 2.3 ± 0.1 Gy/min at phantom surface, respectively.

The normalized central axis lateral and longitudinal dose profiles obtained with MC are presented in Fig. 3. The MC dose profiles were compared against the profiles obtained with GC films for all field sizes. Overall, the MC calculations were in good agreement with the measurements data. The main dose differences between the MC and GC in both directions for 20x20 mm^2 and 10x10 mm^2 beam sizes were within 5 % and located in the low dose tail regions of the profiles.

The simulated and measured depth dose curves for 40x40 mm^2 were shown in Fig. 4: the dose was normalized at the phantom surface and a good agreement was obtained between MC and GC films with a maximum difference of 3.8 %. The comparison of the FWHM and geometric penumbra values of measured and simulated central axis dose profiles were presented in Table 1. The MC FWHM and penumbra values indicated an excellent agreement with GC films with a maximum absolute discrepancy of 0.24 mm and 0.90 mm, respectively.

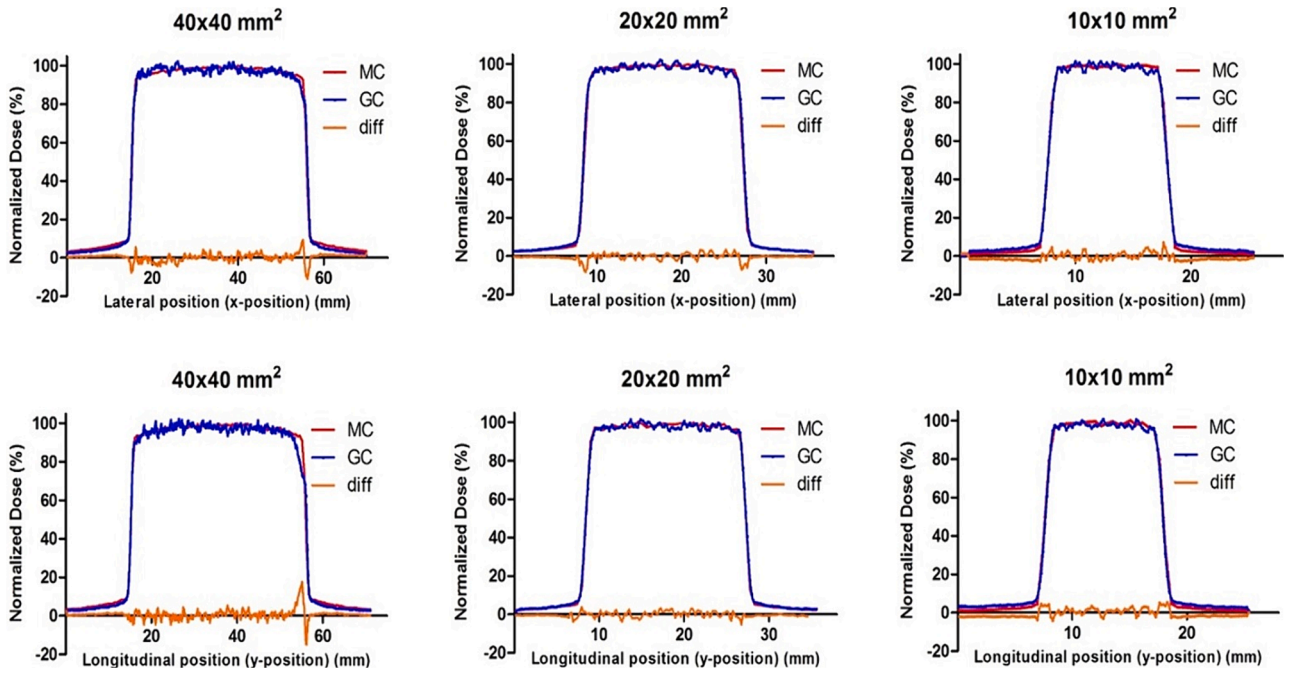

Fig. 3. Comparison between the normalized dose profiles obtained with MC simulations and the corresponding profiles obtained from GC films for all fields in both lateral and longitudinal directions.

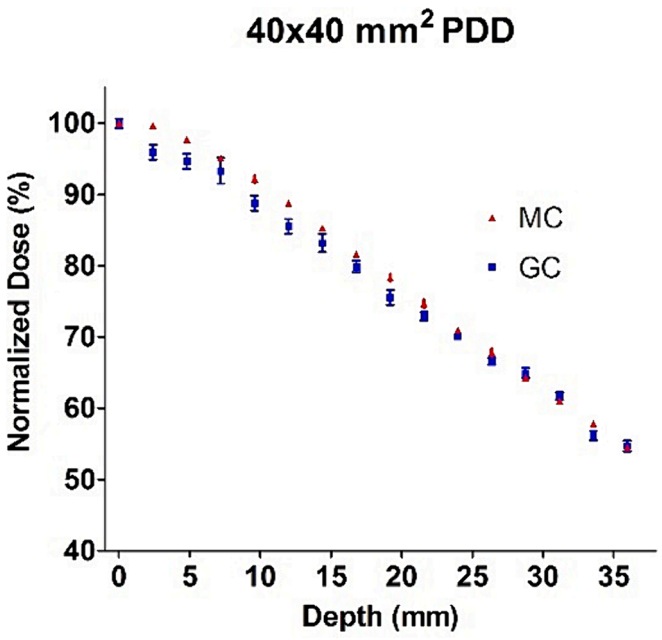

Fig. 4. The plot shows the measured and simulated percentage depth dose for the 40x40 mm^2 open field.

3.2. MC simulations of MB and measurements using GC films

The dose distributions of minibeams at the PMMA phantom surface measured using GC film and simulated with TOPAS MC were shown in Fig. 5-A and Fig. 6-A, respectively. The measured and simulated central axis dose profiles were presented in Fig. 5-B and Fig. 6-B, respectively. As shown in Fig. 5-B, the differences of the peak values along the measured dose profile were approximately 10 % and the valley values were homogenous. The simulated dose profiles with homogeneous peaks and valleys were calculated, as shown in Fig. 6-B.

Table 2 summarizes the measured and simulated dosimetric parameters of the minibeams at the phantom surface. A good agreement was observed between MC and GC data in terms of average-output factor, FWHM, and distance between peaks. The measured and simulated PVDR values at the phantom surface were found to be 13.36 ± 0.32 and 19.56 ± 1.25, respectively.

To investigate the dependence of the minibeams dosimetric features with respect to depth, the PVDR, peak PDD and FWHM were measured at different phantom depths and compared with those calculated by MC simulations. Both simulated and measured PVDR showed a similar pattern, decreasing exponentially with depth, as shown in Fig. 8-A. The simulated PVDR values for each depth were higher than measured PVDR values. This discrepancy was probably due to a non-uniform thickness and/or not perfect alignment of the collimator septa resulting in a slightly higher X-ray absorption. PVDR values obtained in both simulations and measurements were also normalized to the mean entrance PVDR value (Fig. 8-B). The normalized PVDR values calculated by MC were consistent with those measured with GC films; more precisely the normalized PVDR values obtained from measurements were 58.6 ± 2.1 %, 47.9 ± 3.4 %, and 36.5 ± 2.7 % at 9.6 mm, 21.5 and 31.2 mm, respectively.

The peak-PDD curve calculated using MC code has good agreement with the measured peak-PDD curve and the relative differences were 3 % at most (Fig. 7-C). The peak dose dropped to 52.14 ± 1.53 % of surface value at approximately 26 mm depth. The measured FWHM increased up to 0.8 ± 0.01 mm and at 35.9 mm of depth because of the beam divergence and the simulated FWHM at same depth was found to be 0.75 ± 0.02 mm (Fig. 7-D). All the simulated FWHM values as a function of depth demonstrated a satisfactory agreement with GC films.

3.3. In vivo conventional and MBRT of a glioma preclinical model

In order to compare MBRT with open beam RT treatment survival curves were calculated. Survival curves presented in Fig. 8 showed a similar survivor percentage for the MBRT and open beam RT group. The curves were compared using the Log-rank test and the resulting p-value was equal to 0.71. The p-value calculated using the Log-rank test between the control and MBRT curves was equal to 0.003 and, thus, are statistically significantly different.

Table 1
The table shows a comparison of the FWHM and penumbra values for the measured and simulated central axis lateral dose profiles.

Field size (mm^2)	FWHM (mm)			Penumbra (mm) (left-direction)			Penumbra (mm) (right-direction)		
	GC	MC	Difference	GC	MC	Difference	GC	MC	Difference
x-position									
40x40	41.01	40.76	−0.24	0.97	1.01	0.04	0.99	1.02	0.03
20x20	18.99	18.85	−0.14	0.77	0.80	0.04	0.81	0.79	−0.02
10x10	10.30	10.33	0.03	0.75	0.77	0.02	0.84	0.77	−0.07
y-position									
40x40	40.99	40.76	−0.23	0.90	0.99	0.09	1.93	1.02	−0.91
20x20	18.90	18.86	−0.04	0.87	0.79	−0.08	0.87	0.80	−0.07
10x10	10.23	10.32	0.09	0.76	0.79	0.03	0.75	0.76	0.01

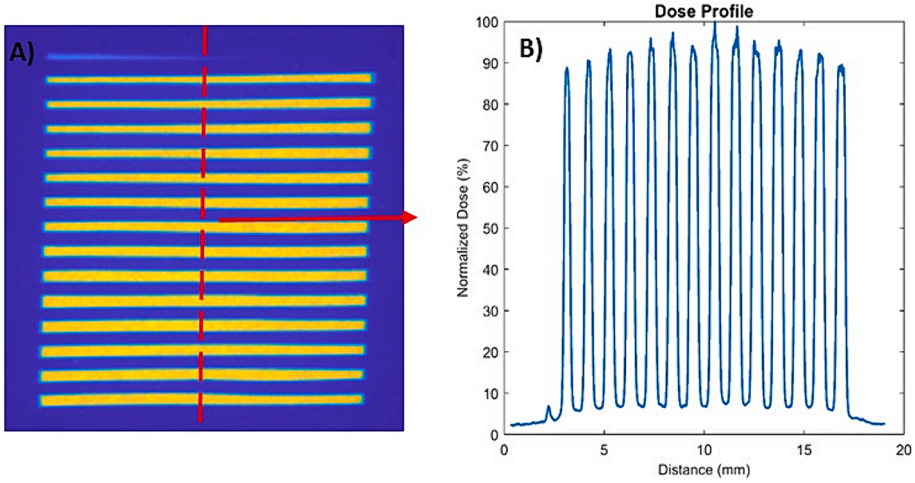

Fig. 5. A) Dose distributions of minibeams measured by GC at the PMMA phantom surface. B) Central axis dose profile. The values were normalized to the maximum value.

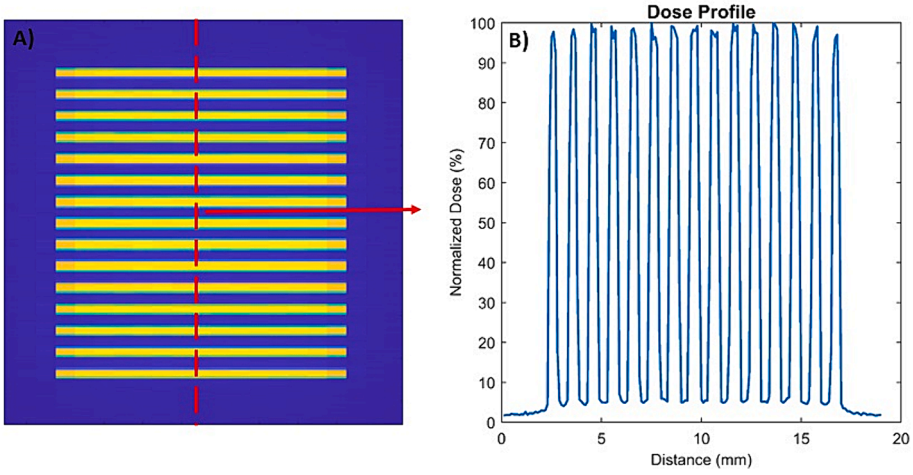

Fig. 6. A) Dose distributions of minibeams simulated by TOPAS at the PMMA phantom surface. B) Central axis dose profile. The values were normalized to the maximum value.

Table 2
The dosimetric characteristics of the minibeam collimator. All values were obtained from the measurements at the phantom surface.

	GC	MC
FWHM of beam (mm)	0.43 ± 0.03	0.47 ± 0.01
Distance between peaks (mm)	1.1 ± 0.05	1.09 ± 0.04
Peak-valley dose ratio	13.4 ± 0.3	19.6 ± 1.3
Average-output factor	0.41 ± 0.01	0.42 ± 0.02

The results concerning acute radiation toxicity are presented in Fig. 9: a large fraction (72 %) of the mice treated with broad beam RT experienced severe damage and 14 % moderate or mild damages. The MBRT group does not present any skin or leg damage.

4. Discussion

The main aim of this study was to design and realize a MB collimator that could easily fit into a commercial image guided small animal irradiator (X-RAD225Cx SmART). We developed a prototype of a compact

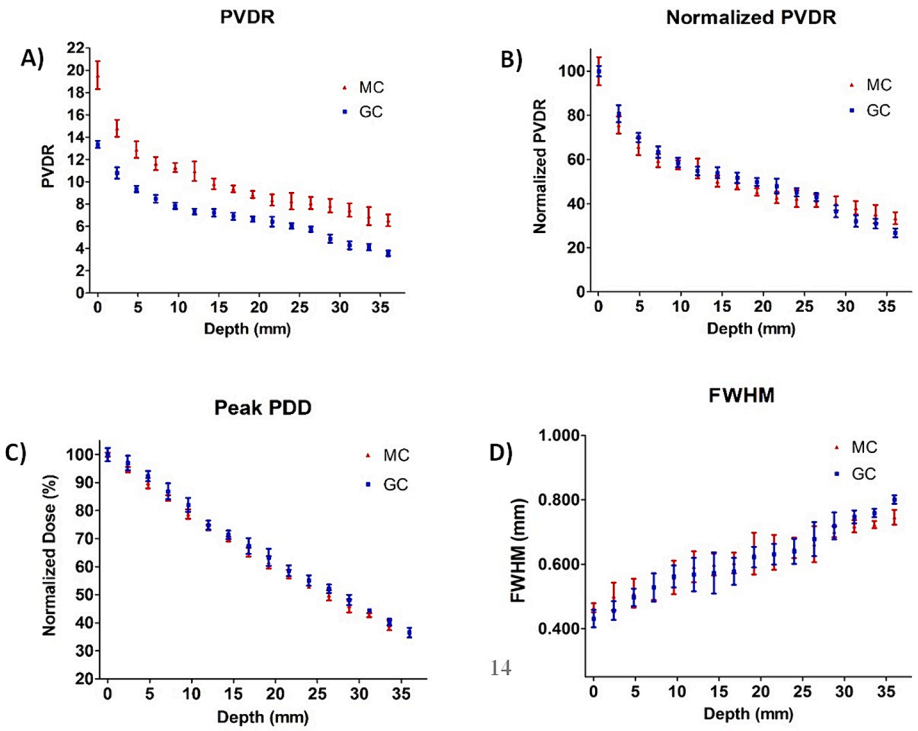

Fig. 7. A) PVDR, B) Normalized to the entrance PVDR, C) Peak PDD, and D) FWHM values at different depths of phantom measured and simulated for mini-beam collimator.

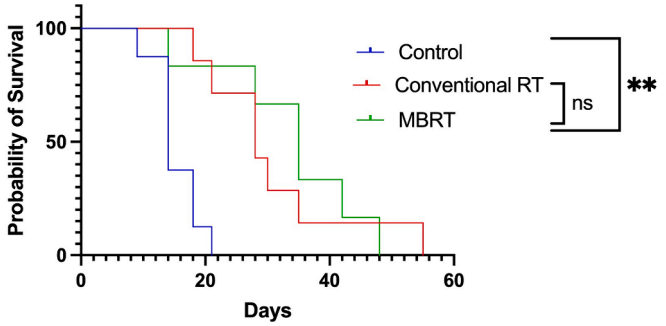

Fig. 8. Survival curves for the control, MBRT and broad beam RT groups. As can be seen the curve of the MBRT is similar to the conventional RT group. The two curves were compared using the Log-rank test and the resulting p value was equal to 0.71. The p value calculated using the Log-rank test between the control and MBRT curves was equal to 0.003.

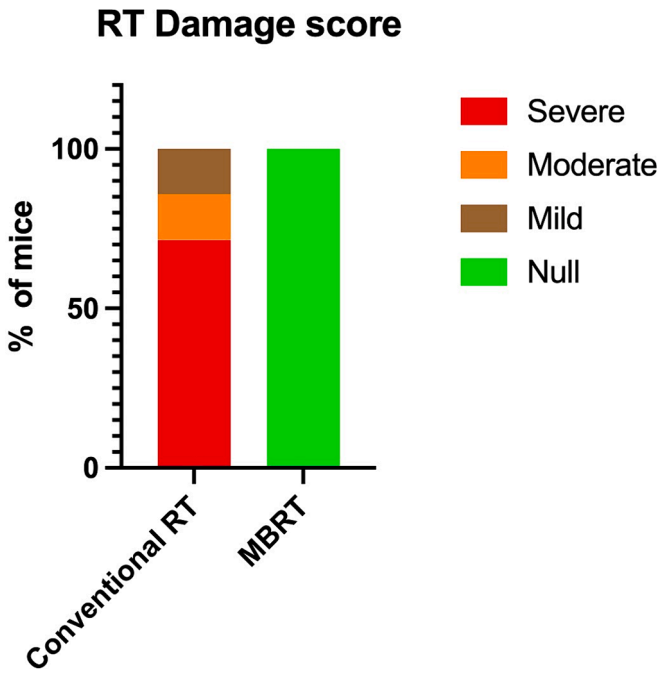

Fig. 9. Acute radiation damage after RT, the plot shows that a large fraction (71%) of the mice treated with broad beam RT experienced severe damages while the MBRT group does not present any skin or leg damage.

secondary minibeam collimator that can be attached to any standard collimator of the SMART system and used at any gantry angle. The dosimetric features of the resulting minibeams were investigated with measurements and MC simulations.

We first developed and validated an MC model of our small animal irradiator for conventional preclinical RT using GC films. The comparison between dose profiles with different beam dimensions and PDD obtained with MC simulations and GC films was satisfactory. Then, TOPAS was used to characterize the output of a secondary mini beam collimator.

By looking at the 2D dose distributions of minibeams obtained from measurement and MC simulation our prototype collimator was not yet optimal. In particular, some lead slits showed to be tilted (with respect the primary collimator axes) with some variability in thickness. The technical difficultness of such a specific collimator fabrication and set-up errors of measurement is the main causes of the differences between MC and GC PVDR. Importantly, this parameter is highly critical and prone to be affected by the uncertainties mentioned above.

Treibel et al [28] performed MC simulation of both microbeams and minibeams dosimetry, comparing the results with film measurements. The simulated PVDR was much higher than measurements, our findings are thus consistent with this study. Another possible explanation for the difference between the measured and calculated PVDR value is the

uncertainties related to the MBC spacer material composition. We modeled PET sheets as spacers for simulations of our minibeam collimator. Esplen et al [29] investigated the impact of the slit (spacer) materials on PVDR. They indicated that the use of plastic material such as PET results in about 4 % increase in PVDR. The variation of PVDR with depth in our study is comparable to previously reported investigation [19]. In order to reduce the spacer absorption, we are investigating the use of glued cardboard instead of PET.

On the other hand, all the remaining dosimetry parameters were in good agreement, suggesting that the actual prototype is sufficiently robust for making MBRT experiments on cell cultures and/or animals, as demonstrated by our first in-vivo experiment.

As expected, the PVDR decreased with increasing depth due to wider penumbra caused by beam divergence.

To get narrow penumbra, source to collimator distance (SCD) should be maximized while collimator to target distance (CTD) should be minimized. However, increasing the SCD can cause the reduction of dose rate. Bazyar et al [19] measured dose rate in air at focal spot surface distance of 37 cm and found 2.9 Gy/min.

The large beam divergence is also due to beam widening as a function of depth. The peak-PDD pattern in our research shows similar behavior with published results of the study performed with 220 kVp energy [18].

The choice of using parallel geometry was made to simplify the construction and to reduce the costs of the collimator. Using the setup described in this paper our parallel collimator allows a uniform square treatment region of about 1x1 cm^2 at the center. As mentioned before this area is enough to treat tumors in small animals. However, at the moment we are also investigating (with MC simulation) the use of a brass focused collimator [30]. It is important also to remind here that considering the energy of x-rays used for preclinical radiotherapy (typically below 300 keV) the production of secondary particles like neutrons does not take place.

Another interesting option is to assemble an MBRT collimator starting from metal plates combined with 3D-printed plastic plates that can be stacked together as shown in [31]. We are designing an updated version of our collimator following a similar approach in order to easily modify the size of MB peaks and valleys.

In vivo results presented in section 3 show that MBRT provides local tumor control for about three weeks after RT treatment and a similar survival fraction of broad beam radiotherapy. After three weeks the tumor control is reduced compared to the broad beam group.

As presented in the previous section the survival curves of MBRT and open field RT are the same and, thus, considering its lower toxicity MBRT is an interesting treatment option.

Considering also that no acute reaction was observed when using an average dose of 25 Gy the MBRT dose could be likely increased without significant increase of toxicity.

5. Conclusions

In this paper we presented a dosimetric evaluation of our minibeam collimator. This collimator can be easily used with any standard collimator of the small animal irradiator (SMART) allowing to perform MBRT with different beam size. In particular, the dosimetric characterization of the minibeam collimator for preclinical MBRT has been accomplished using both film dosimetry and Monte Carlo simulations using TOPAS.

Further optimization of the collimator design, material and manufacturing procedures are currently in progress with the goal of providing robust tools, based on accurate dosimetry, for *in vitro* and in vivo radiobiological MBRT experiments.

In vivo results obtained using a glioma preclinical model showed no normal tissue damage for the group treated with MBRT, while the mice that received conventional radiotherapy showed severe damages. Interestingly the survival curves of MBRT and conventional RT are the same and, thus, considering its lower toxicity MBRT is a better treatment option.

Declaration of competing interest

The authors declare that they have no known competing financial interests or personal relationships that could have appeared to influence the work reported in this paper.

Acknowledgement

The research leading to these results has received funding from: AIRC under IG 2022, ID. 27336, project PI: Antonello E. Spinelli. PNRR-POC-2022-12376062 project PI: Claudio Fiorino, Co-PI: Antonello E. Spinelli.

References

[1] Citrin DE. Recent Developments in Radiotherapy. N Engl J Med 2017;377(11):1065–75. https://doi.org/10.1056/NEJMra1608986.
[2] Rancati T, Fiorino C. Modelling radiotherapy side effects: Practical applications for planning optimisation, 171–206. CRC Press; 2019.
[3] Fernandez-Palomo C, Fazzari J, Trappetti V, Smyth L, Janka H, Laissue J, et al. Animal Models in Microbeam Radiation Therapy: A Scoping Review. Cancers (Basel) 2020;12(3):527. https://doi.org/10.3390/cancers12030527.
[4] Hopewell JW, Trott KR. Volume effects in radiobiology as applied to radiotherapy. Radiother Oncol 2000;56(3):283–8. https://doi.org/10.1016/s0167-8140(00)00236-x.
[5] Curtis HJ. The use of deuteron microbeam for simulating the biological effects of heavy cosmic-ray particles. Radiat Res Suppl 1967;7:250–7.
[6] Bräuer-Krisch E, Serduc R, Siegbahn EA, Le Duc G, Prezado Y, Bravin A, et al. Effects of pulsed, spatially fractionated, microscopic synchrotron X-ray beams on normal and tumoral brain tissue. Mutat Res 2010;704(1–3):160–6. https://doi.org/10.1016/j.mrrev.2009.12.003.
[7] Dilmanian FA, Button TM, Le Duc G, Zhong N, Peña LA, Smith JA, et al. Response of rat intracranial 9L gliosarcoma to microbeam radiation therapy. Neuro Oncol 2002;4(1):26–38. https://doi.org/10.1093/neuonc/4.1.26.
[8] Fernandez-Palomo C, Chang S, Prezado Y. Should Peak Dose Be Used to Prescribe Spatially Fractionated Radiation Therapy?-A Review of Preclinical Studies. Cancers 2022;14(15):3625. https://doi.org/10.3390/cancers14153625.
[9] Slatkin DN, Spanne P, Dilmanian FA, Gebbers JO, Laissue JA. Subacute neuropathological effects of microplanar beams of x-rays from a synchrotron wiggler. Proc Natl Acad Sci U S A1995;92(19):8783-7. https://dx.doi.org/10.1073/pnas.92.19.8783.
[10] Mukumoto N, Nakayama M, Akasaka H, Shimizu Y, Osuga S, Miyawaki D, et al. Sparing of tissue by using micro-slit-beam radiation therapy reduces neurotoxicity compared with broad-beam radiation therapy. J Radiat Res 2017;58(1):17–23. https://doi.org/10.1093/jrr/rrw065.
[11] Laissue JA, Bartzsch S, Blattmann H, Bräuer-Krisch E, Bravin A, Dalléry D, et al. Response of the rat spinal cord to X-ray microbeams. Radiother Oncol 2013;106(1):106–11. https://doi.org/10.1016/j.radonc.2012.12.007.
[12] Bouchet A, Lemasson B, Le Duc G, Maisin C, Bräuer-Krisch E, Siegbahn EA, et al. Preferential effect of synchrotron microbeam radiation therapy on intracerebral 9L gliosarcoma vascular networks. Int J Radiat Oncol Biol Phys 2010;78(5):1503–12. https://doi.org/10.1016/j.ijrobp.2010.06.021.
[13] Dilmanian FA, Zhong Z, Bacarian T, Benveniste H, Romanelli P, Wang R, et al. Interlaced x-ray microplanar beams: a radiosurgery approach with clinical potential. Proc Natl Acad Sci U S A 2006;103(25):9709–14. https://doi.org/10.1073/pnas.0603567103.
[14] Prezado Y, Deman P, Varlet P, Jouvion G, Gil S, Le Clec'H C, et al. Tolerance to Dose Escalation in Minibeam Radiation Therapy Applied to Normal Rat Brain: Long-Term Clinical. Radiological and Histopathological Analysis Radiat Res 2015;184(3):314–21. https://doi.org/10.1667/RR14018.1.
[15] Prezado Y, Sarun S, Gil S, Deman P, Bouchet A, Le Duc G. Increase of lifespan for glioma-bearing rats by using minibeam radiation therapy. J Synchrotron Radiat 2012;19(Pt 1):60–5. https://doi.org/10.1107/S0909049511047042.
[16] Babcock K, Sidhu N, Kundapur V, Ali K. Collimator design for experimental minibeam radiation therapy. Med Phys 2011;38(4):2192–7. https://doi.org/10.1118/1.3560425.
[17] Hadsell M, Zhang J, Laganis P, Sprenger F, Shan J, Zhang L, et al. A first generation compact microbeam radiation therapy system based on carbon nanotube X-ray technology. Appl Phys Lett 2013;103(18):183505. https://doi.org/10.1063/1.4826587.
[18] Prezado Y, Dos Santos M, Gonzalez W, Jouvion G, Guardiola C, Heinrich S, et al. Transfer of Minibeam Radiation Therapy into a cost-effective equipment for radiobiological studies: a proof of concept. Sci Rep 2017;7(1):17295. https://doi.org/10.1038/s41598-017-17543-3.
[19] Bazyar S, Inscoe CR, O'Brian ET, Zhou O, Lee YZ. Minibeam radiotherapy with small animal irradiators; in vitro and in vivo feasibility studies. Phys Med Biol 2017;62(23):8924–42. https://doi.org/10.1088/1361-6560/aa926b.

[20] Fontanarosa D, Benitez J, Talkhani S, et al. A novel add-on collimator for preclinical radiotherapy applications using a standard cell irradiator: design, construction, and validation. Med Phys 2020;47(6):2461–71. https://doi.org/10.1002/mp.14110.
[21] Ma CM, Coffey CW, DeWerd LA, Liu C, Nath R, Seltzer SM, et al. American Association of Physicists in Medicine. AAPM protocol for 40–300 kV x-ray beam dosimetry in radiotherapy and radiobiology. Med Phys 2001;28(6):868–93. https://doi.org/10.1118/1.1374247.
[22] Spinelli AE, D'Agostino E, Broggi S, Claudio F, Boschi F. Small animal irradiator dose distribution verification using radioluminescence imaging. J Biophotonics 2020;13(7):e201960217.
[23] Perl J, Shin J, Schümann J, et al. TOPAS: An innovative proton Monte Carlo platform for research and clinical applications. Med Phys 2012;39(11):6818–37. https://doi.org/10.1118/1.4758060.
[24] Poludniowski G, Evans PM. Calculation of x-ray spectra emerging from an x-ray tube. Part I. Electron penetration characteristics in x-ray targets. Med Phys 2007;34:2164–74. https://doi.org/10.1118/1.2734725.
[25] Poludniowski G. Calculation of x-ray spectra emerging from an x-ray tube. Part II. X-ray production and filtration in x-ray targets. Med Phys 2007;34:2175–86. https://doi.org/10.1118/1.734726.
[26] Poludniowski G, Landry G, DeBlois F, et al. SpekCalc: a program to calculate photon spectra from tungsten anode x-ray tubes. Phys Med Biol 2009;54:N433–8. https://doi.org/10.1088/0031-9155/54/19/N01.
[27] Soto LA, Casey KM, Wang J, Blaney A, Manjappa R, Breitkreutz D, et al. FLASH Irradiation Results in Reduced Severe Skin Toxicity Compared to Conventional-Dose-Rate Irradiation. Radiat Res 2020;194(6):618–24. https://doi.org/10.1667/RADE-20-00090. Erratum. In: Radiat Res. 2022 Feb 1;197(2):207.
[28] Treibel F, Nguyen M, Ahmed M, Dombrowsky A, Wilkens JJ, Combs SE, et al. Establishment of Microbeam Radiation Therapy at a Small-Animal Irradiator. Int J Radiat Oncol Biol Phys 2021;109(2):626–36. https://doi.org/10.1016/j.ijrobp.2020.09.039.
[29] Esplen NM, Chergui L, Johnstone CD, Bazalova-Carter M. Monte Carlo optimization of a microbeam collimator design for use on the small animal radiation research platform (SARRP). Phys Med Biol 2018;63(17):175004. https://doi.org/10.1088/1361-6560/aad7e2.
[30] Guardiola C, Peucelle C, Prezado Y. Optimization of the mechanical collimation for minibeam generation in proton minibeam radiation therapy. Med Phys 2017;44(4):1470–8. https://doi.org/10.1002/mp.12131.
[31] Stengl C, Arbes E, Thai LJ, et al. Development and characterization of a versatile mini-beam collimator for pre-clinical photon beam irradiation. Med Phys 2023;50(8):5222–37. https://doi.org/10.1002/mp.16432.